Discovery of fissionogenic Cs and Ba capture five years after Oklo reactor shutdown

Evan E. Groopman[a,1], David G. Willingham[a], Alex P. Meshik[b], and Olga V. Pravdivtseva[b]

[a]Materials Science and Technology Division, US Naval Research Laboratory, Washington, DC 20375; and [b]Physics Department, Washington University in St. Louis, St. Louis, MO 63130

Edited by Mark H. Thiemens, University of California at San Diego, La Jolla, CA, and approved July 9, 2018 (received for review April 26, 2018)

Understanding the release and sequestration of specific radioactive signatures into the environment is of extreme importance for long-term nuclear waste storage and reactor accident mitigation. Recent accidents at the Fukushima and Chernobyl nuclear reactors released radioactive ^{137}Cs and ^{134}Cs into the environment, the former of which is still live today. We have studied the migration of fission products in the Oklo natural nuclear reactor using an isotope imaging capability, the NAval Ultra-Trace Isotope Laboratory's Universal Spectrometer (NAUTILUS) at the US Naval Research Laboratory. In Oklo reactor zone (RZ) 13, we have identified the most depleted natural U of any known material with a ^{235}U/^{238}U ratio of 0.3655 ± 0.0007% (2σ). This sample contains the most extreme natural burnup in ^{149}Sm, ^{151}Eu, ^{155}Gd, and ^{157}Gd, which demonstrates that it was sourced from the most active Oklo reactor region. We have discovered that fissionogenic Cs and Ba were captured by Ru metal/sulfide aggregates shortly following reactor shutdown. Isochrons from the Ru aggregates place their closure time at 4.98 ± 0.56 y after the end of criticality. Most fissionogenic ^{135}Ba and ^{137}Ba in the Ru migrated and was incorporated as Cs over this period. Excesses in ^{134}Ba in the Ru point to the burnup of ^{133}Cs. Cesium and Ba were retained in the Ru despite local volcanic activity since the reactor shutdown and the high level of activity during reactor operation.

Oklo | SIMS | AMS | isotope imaging | natural fission reactor

Two billion years ago, an incredible confluence of conditions yielded 17 sites in central Africa where natural nuclear fission reactors operated over periods of 24 ka to 1 Ma, known as the Oklo phenomenon (e.g., refs. 1–5 and references therein). To sustain fission, anthropogenic reactors require uranium fuel to be enriched in its main fissile isotope, ^{235}U, from its present-day abundance of 0.72%. Two billion years ago, the abundance of ^{235}U was naturally higher, ∼3%, due to the shorter half-life of ^{235}U ($t_{1/2}$ = 0.7 Ga) relative to ^{238}U ($t_{1/2}$ = 4.5 Ga). This, combined with large deposits of uranium ore and groundwater as a neutron moderator, allowed nuclear fission to occur underground, with the reactors cycling on for 30 min and off for 2.5 h over tens of thousands of years (6). These reactor zones (RZs) provide analogs for the study of long-term nuclear waste storage. Each site experienced a different duration of pulsed fission and was subject to varied postfission processing, such as terrestrial weathering at sites near the surface or local volcanic intrusions. The periodic intrusion of groundwater not only moderated the reactors, but also removed fission products. To enable better nuclear waste storage, it is important to understand how radioactive fission products of different elements migrate from or are retained in the nuclear fuel. For instance, secondary La–Ce–Sr–Ca aluminous hydroxy phosphate (phosphate) minerals in Oklo RZ 13 (7) were found to have captured radiogenic Xe in quantities greater than those found in any other terrestrial mineral, while very little Xe was retained in the uraninite (UO_2) fuel (8). Cesium, which is one of the most volatile elements, is also incompatible with the UO_2 structure, limiting its retention within the reactor fuel (9). Cesium migrated to grain boundaries and was mostly lost from the Oklo reactors (9, 10); in anthropogenic reactors, it becomes trapped between the nuclear fuel and the reactor cladding, which heightens the risk of instantaneous release if a storage cask were ruptured (11). Several radioactive Cs isotopes result from fission or burnup of ^{133}Cs, including ^{134}Cs ($t_{1/2}$ = 2.1 y), ^{135}Cs ($t_{1/2}$ = 2.3 Ma), and ^{137}Cs ($t_{1/2}$ = 30.2 y) (Fig. 1). These comprise >10% of the total fission yield, creating a problem for both short- and long-term storage. There has been considerable work done mapping the spread and retention of fissionogenic Cs in soils, sediments, plants, and animals following the Fukushima and Chernobyl reactor accidents due to health and environmental concerns (e.g., refs. 12 and 13 and references therein).

Oklo RZ 13 is one of the best-preserved zones, making it a close natural analog to long-term nuclear waste storage and an ideal sample in which to study retention and migration of fission products (3, 7). In addition, large samples (several millimeters) from the different RZs may be easily studied, as they are no longer radioactive, which allows for thorough investigation of heterogeneities across the samples.

Results

We studied the spatial distribution and isotopic abundances of fission and neutron capture products in a sample from drill hole S2 in gallery SD.37 of Oklo RZ 13 (6–8) using the NAval Ultra Trace Isotope Laboratory's Universal Spectrometer (NAUTILUS) at the US Naval Research Laboratory (NRL). NAUTILUS is a combination secondary ion mass spectrometer (SIMS) and single-stage accelerator mass spectrometer (SSAMS), which enables the micrometer-scale and molecular-isobar-free analysis of samples in situ (14–16). NAUTILUS provides a state-of-the-art, direct, molecule-free isotope imaging capability over regions 10–500 μm in

Significance

The Oklo natural nuclear reactors provide a wealth of information regarding the migration and retention of fission products in nuclear wastes. Radioactive volatile and gaseous elements easily escape from reactor fuel into the environment without proper containment. Cesium, in particular, represents a significant environmental and health hazard. Here, we used an isotope imaging system to identify the location of sequestered fissionogenic Cs and Ba in Oklo. Cesium and Ba were captured in Ru metal/sulfide aggregates shortly after reactor criticality ceased. These elements were otherwise nearly completely lost from the reactor. We have further discovered the most depleted natural U on Earth, indicating that these fission products were retained in the most active region of the reactor.

Author contributions: E.E.G., D.G.W., A.P.M., and O.V.P. designed research; E.E.G. performed research; E.E.G. contributed new reagents/analytic tools; E.E.G. and D.G.W. analyzed data; and E.E.G. wrote the paper.

The authors declare no conflict of interest.

This article is a PNAS Direct Submission.

Published under the PNAS license.

[1]To whom correspondence should be addressed. Email: evan.groopman@nrl.navy.mil.

This article contains supporting information online at www.pnas.org/lookup/suppl/doi:10.1073/pnas.1807267115/-/DCSupplemental.

Published online August 13, 2018.

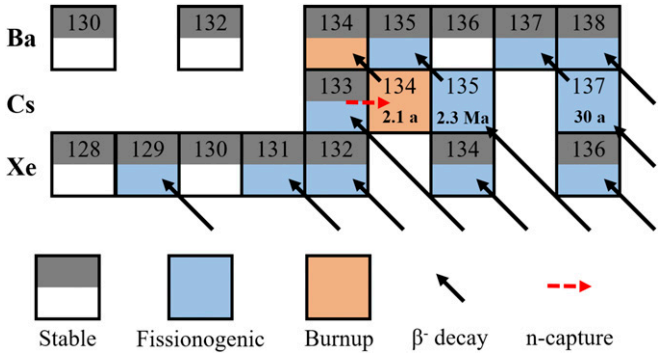

Fig. 1. The fissionogenic and n-capture isotopes of Ba, Cs, and Xe are shown with β^- decay pathways. Isotopes with half-lives >2 wk are shown. Barium has three stable fissionogenic isotopes. Its other isotopes are shielded by Xe and have negligible fission yields. Barium-134 is enhanced by n-capture on ^{133}Cs. Adapted from ref. 25, with permission from Elsevier.

size for the study of heterogeneous materials with high sensitivity and signal-to-noise. Molecular isobars are ordinarily detrimental to mass spectrometry analyses, especially when measuring trace, high-mass elements, such as the actinides and fission products, and in perturbed isotopic systems where corrections cannot be reliably made. Considerable isotopic work on the Oklo and Bangombé reactors has been performed to date [De Laeter and Hidaka (2) and references therein], including bulk studies by isotope dilution (ID) inductively coupled plasma mass spectrometry (ICP-MS) and ID thermal ionization mass spectrometry, in addition to in situ studies by laser ablation ICP-MS and traditional SIMS. We present the results of NAUTILUS measurements which are inaccessible to other mass-spectrometric techniques.

We measured the most depleted natural U on Earth, to our knowledge, in uraninite grains from RZ 13 with ^{235}U/^{238}U ratios as low as 0.3655 ± 0.0007% (2σ) [present-day natural ^{235}U/^{238}U = 0.7255% (17)]. Across the 3- × 4-mm sample, ^{235}U/^{238}U varied grain-to-grain, ranging up to 0.396%. This compares to ^{235}U/^{238}U ratios of, for example, 0.465% in RZ 2, 0.694% in RZ 3, 0.559% in RZ 9, 0.507% in RZ 10, 0.463% in bulk RZ 13 (0.38% in the core), and 0.662% in Bangombé from earlier work (3–5, 18, 19). The gradient in ^{235}U/^{238}U that we observed across our 4-mm sample qualitatively agrees with ^{235}U/^{238}U ranging up to 0.5–0.6% across the ∼30-cm-thick core of RZ 13 (3). This suggests that our sample was located at the most active region of all RZs and that the neutron flux in RZ 13 was heterogeneous and/or not well thermalized (20).

Conventional SIMS cannot measure trace high-mass and rare earth element (REE) isotope abundances in samples with complex and large molecular backgrounds (e.g., any mineral) and with nonnormal isotope ratios. NAUTILUS makes direct measurements of these isotopes by dissociating molecular isobars and forgoing deconvolution (Fig. 2) (14–16, 21–23). Knowledge of fission and n-capture product isotope abundances from the Oklo RZs to this point has predominantly come from bulk ID measurements, with some in situ SIMS work of secondary minerals. Hidaka and Holliger (4) provide a comprehensive account of such abundances; De Laeter and Hidaka (2) provide a review of mass spectrometry applied to Oklo. From direct in situ measurements of uraninites in RZ 13, we found that several isotopes with large n-capture cross-sections were more depleted than those reported by Hidaka and Holliger (4) (*SI Appendix*, Table S1), with ^{151}Eu/^{153}Eu = 0.2606 ± 0.0020 (2σ) and ^{149}Sm/^{147}Sm = 0.004849 ± 0.000046 (2σ) (normal ^{151}Eu/^{153}Eu = 0.916 and ^{149}Sm/^{147}Sm = 0.922) (see Figs. 2 and 3 for SIMS vs. SIMS+SSAMS comparison). Gadolinium (Gd)-155 and Gd-157 were depleted essentially to zero, with their measured ion signals being equivalent to a 4‰ addition of normal Gd relative to ^{160}Gd, or smaller than the error of the measurement. A small component of spontaneous fission or ingrowth following reactor operation could also be present. Therefore, we could not directly compare ^{155}Gd/^{156}Gd and ^{157}Gd/^{158}Gd ratios to earlier work; however, the ^{156}Gd/^{160}Gd and ^{158}Gd/^{160}Gd ratios we measured were 6.96 ± 0.08 (2σ) and 3.40 ± 0.04 (2σ), respectively, 40% and 20% more enriched than those in Hidaka and Holliger (4) (normal ^{156}Gd/^{160}Gd = 0.936, ^{158}Gd/^{160}Gd = 1.14). This enrichment pattern in burnup products ^{156}Gd and ^{158}Gd relative to ^{160}Gd, which has no fission or n-capture contribution, is consistent with a system where ^{155}Gd and ^{157}Gd were continuously depleted to zero. We expect the enrichment in ^{156}Gd/^{160}Gd to be larger than that in ^{158}Gd/^{160}Gd since ^{155}Gd has several pathways for replenishment during reactor operation—for example, fission yield and the reactions ^{153}Eu(n,γ)^{154}Eu(n,γβ$^-$)^{155}Gd—while ^{157}Gd is only replenished by fission. Europium (Eu)-154 and Eu-155 have half-lives of 8.6 and 4.8 y, respectively, and thermal n-capture cross-sections of >1 kb; ^{153}Eu is stable with a cross-section of 300 b and a resonance integral of 1.4 kb (24). Furthermore, ^{156}Gd has an additional enhancement pathway ^{155}Eu(n, γβ$^-$)^{156}Gd, while ^{158}Gd does not. The phosphate was similarly depleted/enriched in its Gd isotopes, although Gd and other heavy REEs were less abundant than in the uraninite (*SI Appendix*, Table S1). Dysprosium isotopes 161–164, which all have appreciable n-capture cross-sections and resonance integrals, were measured in uraninite as well, with significant depletions found in the ^{161,162,164}Dy/^{163}Dy ratios of 40%, 22%, and 77% relative to normal. The phosphate composition was 6–9% less depleted in each isotope ratio relative to the uraninite. Since Dy isotopes have negligible fission yield, they act as a neutron fluence monitor, from which we estimated a fluence of 7.7 × 10^{20} n•cm^{-2}, in line with earlier work (4).

Understanding the behavior of radiogenic Cs in modern reactors is important since two fissionogenic isotopes, ^{135}Cs and ^{137}Cs, each comprise ∼6–6.5% of the total fission yield, with half-lives of 2.3 Ma and 30.2 y, respectively. They decay to the stable isotopes ^{135}Ba and ^{137}Ba, respectively (Fig. 1). Cesium is mobile, and ^{137}Cs accounts for a major portion of reactor waste activity on the timescale of several generations, while ^{135}Cs remains active long after. Earlier bulk isotopic work identified the presence of radiogenic Ba within the RZs, indicating that differentiation between Ba and Cs occurred on the order of 20 y following criticality and that fissionogenic ^{135}Ba and ^{137}Ba chemically behaved as Cs (9, 25, 26).

Using raster ion imaging on the NAUTILUS, we discovered several "hotspots" containing large abundances of fissionogenic ^{134}Ba, ^{135}Ba, ^{137}Ba, and ^{138}Ba (denoted with *), correlated with ^{133}Cs (Fig. 4). Barium-134* was from n-capture on ^{133}Cs; ^{135}Ba*

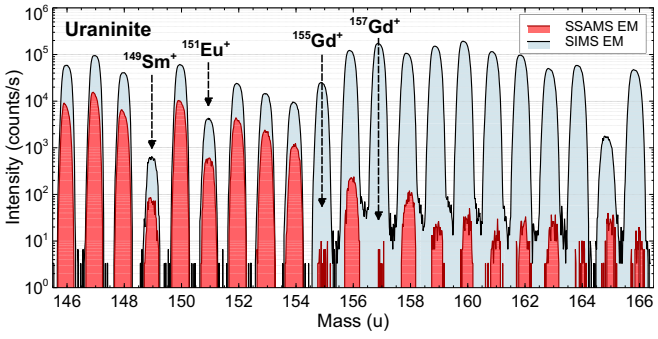

Fig. 2. Mass scan comparison (charge, z = +1) over the mid-REEs to heavy REEs measured on the SIMS (blue) and SSAMS (red) EM detectors of NRL's NAUTILUS. The SSAMS mass scan illustrates the removal of the intense molecular background visible in the SIMS, allowing for direct measurement of fission products and n-capture depletions. The SIMS spectrum cannot be deconvolved by using conventional energy filtering methods because the isotopic abundances are nonnormal.

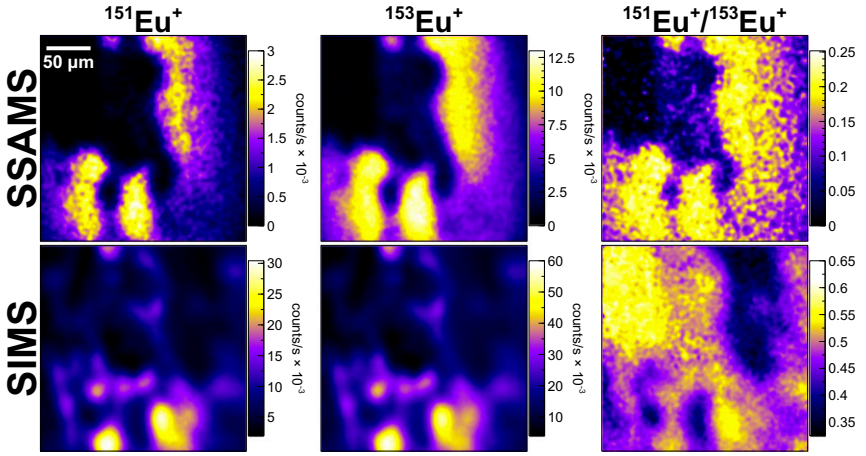

Fig. 3. Europium isotope ratio imaging on the SSAMS (*Upper*; molecule-free) and SIMS (*Lower*) EMs of the NAUTILUS. Europium is concentrated in uraninite and not in aluminous phosphate. Europium-151 is highly depleted due to n-capture (more than ^{153}Eu), but this is obscured by a large and complex molecular background on the SIMS. The SIMS images contain many false-positive features, and the isotope ratio image is in fact nearly the inverse of the true ratio image (^{151}Eu/^{153}Eu$_{normal}$ = 0.916).

and ^{137}Ba* were from the decay of ^{135}Cs* and ^{137}Cs*, respectively; and ^{138}Ba* was from direct fission. The hotspots contain isotope ratios deviating from normal up to δ^{134}Ba = 310‰, δ^{135}Ba = 1830‰, δ^{137}Ba = 1010‰, and δ^{138}Ba = 240‰ (±10‰), with Ba* and Cs abundances generally correlated (Fig. 5 and *SI Appendix*, Table S1); δ^{i}Ba = δ^{i}Ba/^{136}Ba = 1,000 × [(^{i}Ba/^{136}Ba)$_{sample}$/(^{i}Ba/^{136}Ba)$_{normal}$ − 1)]. Without molecule-free imaging, these regions would be nearly impossible to locate given the large molecular background at each nominal mass. Barium and Cs in the phosphate had nearly normal isotopic composition, which significantly impacted imaging contrast and necessitated the use of direct isotope ratio imaging (Fig. 4). The uraninite showed Ba* excesses up to 1%, but with vastly lower Cs and Ba abundances than the phosphate. The hotspots of Ba* were found to be localized within Ru metal aggregates and sulfides, one of which was found completely entrained within a uraninite grain (Fig. 4), while others were found on grain perimeters or surrounded by phosphate. Gauthier-Lafaye et al. (3) reported that the metallic aggregates tend to consist of Pb–Ru–As–S and Pb–Te phases with galena (PbS) as a secondary phase, with the majority of aggregates in RZ 13 existing between uraninite grains, as we observed. The Ru aggregate pictured in Fig. 4, which was completely encapsulated within uraninite, showed a remarkable difference in its fissionogenic Ba abundances with respect to the intergrain aggregates (diamond marker in Figs. 5 and 6). In plots of the Ba* isotopes and of ^{133}Cs relative to ^{136}Ba (a shielded and essentially non-fissionogenic isotope; Fig. 1), the intergrain Ru aggregates showed near-perfect correlations of all Ba* isotopes with ^{133}Cs, while the inclusion showed markedly higher ^{135,137,138}Ba* relative to ^{133}Cs and no ^{134}Ba*. Since ^{133}Cs is the only stable Cs isotope, it is not typically feasible to distinguish between fissionogenic and primordial components. Earlier work suggested that the ^{133}Cs in Oklo is nearly all fissionogenic (25, 26). The isochrons in Fig. 5 show a clear difference between the intergrain aggregates and the

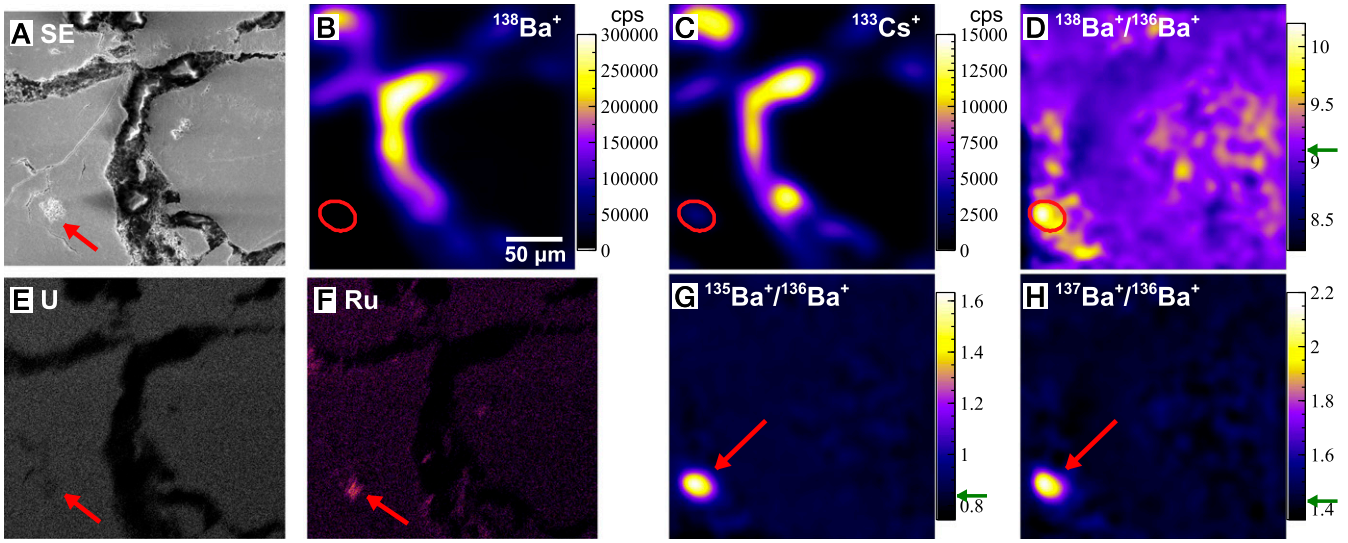

Fig. 4. Molecule-free isotope ratio imaging identified fissionogenic ^{135,137}Ba in a localized spot within a uraninite grain. SEM–energy-dispersive X-ray found this spot to contain Ru metal and sulfides (*E* and *F*). The Ru phases formed ∼5 y after criticality and captured ^{135,137}Cs* in similar abundance. The majority of Ba and Cs is concentrated in aluminous phosphate (*B* and *C*), although it has normal isotopic composition (indicated by green arrows in *D*, *G*, and *H* scale bars). Secondary electron (*A*) and SIMS (*B*–*D*, *G*, and *H*) images are shifted horizontally relative to each other by ∼50 μm.

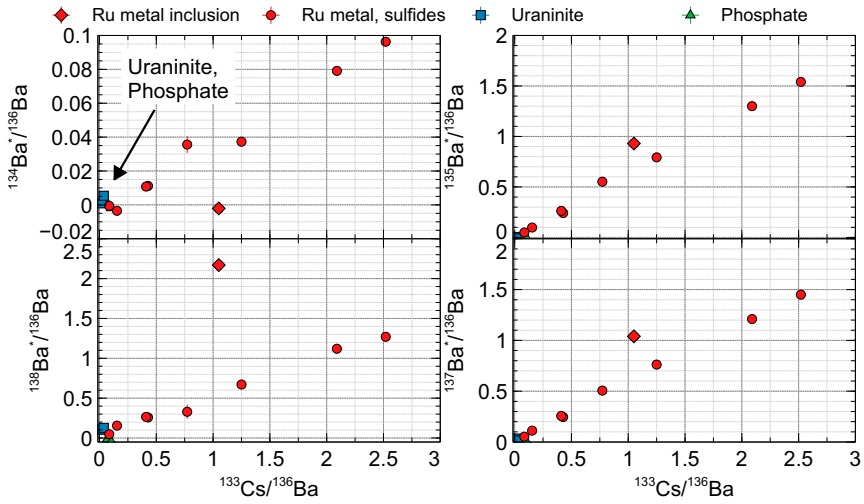

Fig. 5. Fissionogenic Ba and Cs relative to ^{136}Ba. Uraninite and aluminous phosphate show almost no retained Ba*, while Ru aggregates between uraninite grains show highly correlated Ba* and Cs (circles). The Ru inclusion within a uraninite grain (diamond) is an outlier, reflecting the fractionation of Cs between uraninite and the interuraninite mineral phases.

included Ru grain, indicating fractionation in ^{133}Cs. This is especially apparent in the plot of ^{134}Ba*/^{136}Ba, since ^{134}Ba* is a burnup product of ^{133}Cs. The ^{133}Cs was apparently not retained within the uraninite long enough for ^{134}Cs to be produced by n-capture and subsequently sequestered in the Ru inclusion. For the intergrain aggregates, however, the correlation between ^{134}Ba* and ^{133}Cs indicated that ^{134}Cs ($t_{1/2}$ = 2.1 y) was live during Ru formation.

An isochron of ^{135,137}Ba* was constructed relative to ^{138}Ba* to remove uncertainty with respect to the relative Ba/Cs SIMS ion yield and fractionation or loss of ^{133}Cs (Fig. 6*A*). The Ru metal inclusion was collinear with the other Ru aggregates in this parameterization, so it shared an age relationship. Since the ^{235}U fission yields of ^{133}Cs, ^{135}Cs, ^{137}Cs, and ^{138}Ba were all similar (6.7%, 6.6%, 6.2%, and 6.8%, respectively), and with comparable abundances of ^{135}Ba* and ^{137}Ba* in the Ru grains, we deduced qualitatively that closure occurred within the lifetime of ^{137}Cs following criticality based upon the large difference in ^{135,137}Cs half-lives, in agreement with refs. 25 and 26. Therefore, ^{135}Ba* and ^{137}Ba* must have migrated as Cs before capture. Fig. 6*A*, relating ^{137}Ba*/^{138}Ba* vs. ^{135}Ba*/^{138}Ba*, depicts a slope of ^{137}Ba*/^{135}Ba* = 0.858 ± 0.018 and an intercept of ^{137}Ba*/^{138}Ba* = 0.113 ± 0.012. The low abundance of ^{138}Ba* in some of the Ru aggregates was responsible for the larger error ellipses. The isochron slope yielded an age of $4.16^{+0.92}_{-0.90}$ y using Eq. **1**:

$$\left(\frac{^{137}Cs^*}{^{135}Cs^*}\right)_{init} = \left(\frac{Cs_{137f}}{Cs_{135f}}\right) \times \frac{e^{-\lambda_{137}t}}{e^{-\lambda_{135}t}}, \qquad [1]$$

where Cs_{if} is the fission yield for isotope i (Cs_{137f}/Cs_{135f} = 0.943). This agreed with an age estimate of $5.79^{+0.66}_{-0.65}$ y from the ^{137}Ba*/^{138}Ba* intercept of Fig. 6*A* using Eq. **2**:

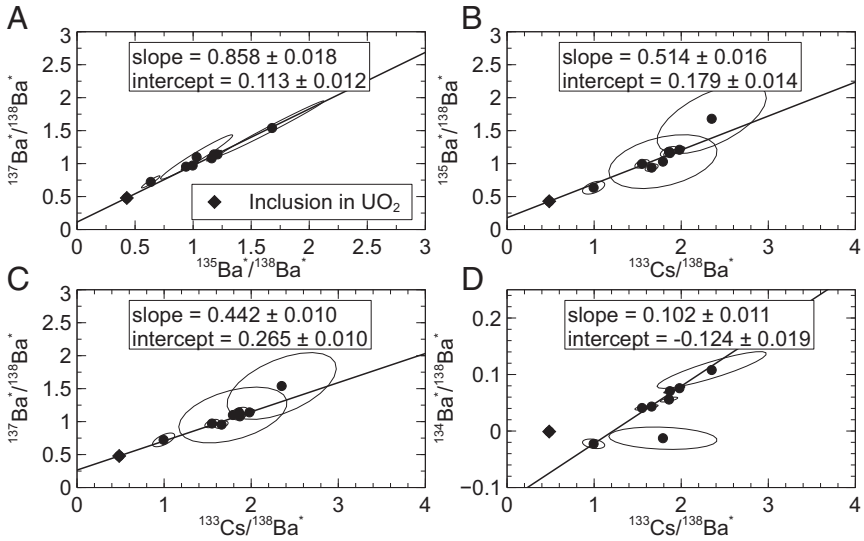

Fig. 6. Isochrons of fissionogenic Ba and Cs from Ru aggregates. The slope and intercept of the ^{137}Ba*/^{138}Ba* vs. ^{135}Ba*/^{138}Ba* isochron (*A*) yields a mean formation age of 4.98 ± 0.56 y following reactor shutdown and illustrates that Ba* behaved predominantly as Cs before incorporation. The Ru grain included in uraninite is shown as a diamond; interuraninite Ru aggregates are shown as circles (as in Fig. 5). The ^{135}Ba*/^{138}Ba* intercept (*B*) indicates that Cs was lost after formation, likely during the intrusion of a dolerite dike ∼1 Ga after shutdown. The ^{137}Ba*/^{138}Ba* intercept (*C*) is similarly compromised. Excess ^{134}Ba indicates the burnup of ^{133}Cs near the intergrain aggregates, although the abundance appears fractionated (*D*).

$$\left(\frac{^{137}Ba^*}{^{138}Ba^*}\right)_{init} = \left(\frac{Cs_{137f}}{Ba_{138f}}\right) \times \left(1 - e^{-\lambda_{137}t}\right), \quad [2]$$

where $Cs_{137f}/Ba_{138f} = 0.965$. From these two estimates, we derived a mean formation age of 4.98 ± 0.56 y for the Ru aggregates following reactor shutdown. We assumed that Cs was being continuously lost from the uraninite during reactor operation since Cs is not compatible with the uraninite matrix (9). Our estimate was shorter than the 20-y timescale previously postulated (25). The isochrons in Fig. 6 *B* and *C* show the $^{135}Ba^*/^{138}Ba^*$ and $^{137}Ba^*/^{138}Ba^*$ ratios relative to $^{133}Cs/^{138}Ba^*$. Similar to the isochrons in Fig. 5, slopes less than $Cs_{135f}/Cs_{133f} = 0.975$ and $Cs_{137f}/Cs_{133f} = 0.920$ indicated an excess of ^{133}Cs relative to the expected fission yield. We assumed that this corresponded to ^{133}Cs produced earlier during reactor operation, since nearly all of the Cs in the Oklo reactor was fissionogenic (25). The $^{135}Ba^*/^{138}Ba^*$ intercept in Fig. 6*B* yielded a nonsensical age of 680,000 y, far longer than the 24,200-y operating time for RZ 13 (3, 4). This was likely due to Cs loss during the intrusion of a dolerite dike ∼850 Ma ago, which would have shifted the isochrons uniformly to the left, increasing the $^{135}Ba^*/^{138}Ba^*$ intercept and the apparent age. The intercept in Fig. 6*C* was similarly compromised by apparent ^{133}Cs loss, so only the isochron in Fig. 6*A*, with no ^{133}Cs dependence, was useful for dating. Despite the posited loss of ^{133}Cs >1 Ga following reactor shutdown, there was no evidence for loss of fissionogenic Ba, which can form stable $BaRuO_4$ (27) and other Ru oxides via cation substitution (28, 29).

The isochron in Fig. 6*D* relating $^{134}Ba^*/^{138}Ba^*$ to $^{133}Cs/^{138}Ba^*$ was more complicated since ^{134}Ba is not produced from the decay of fission products, but from the burnup of ^{133}Cs to ^{134}Cs. The Ru inclusion was excluded from the linear regression. The positive slope (0.102 ± 0.011) of the isochron indicated that ^{134}Cs was live during Ru formation, which agreed with our estimate of a 5-y formation time. The isochron was not useful, however, for estimating the neutron flux because we could not accurately determine fractionation within the system on this timescale or the addition of ^{133}Cs following reactor shutdown. Using the isochron slope, we estimated the neutron flux immediately before reactor shutdown to be 6.8×10^{20} n·cm^{-2}·y^{-1}, a nonsensical value. We assumed a neutron capture cross-section of 28.9 barns and a resonance integral of 446.2 barns (24), a spectral index of 0.241 (4), a temperature of 1,000 K, and the 5-y decay time following reactor shutdown. The large negative intercept on the $^{134}Ba^*/^{138}Ba^*$ axis, which would have been more negative before any Cs loss, is also difficult to explain.

Fractionation between Cs and Ba was likely in the uraninite, given the slopes of $^{135}Ba^*/^{136}Ba$ (0.621 ± 0.011) and $^{138}Ba^*/^{136}Ba$ (0.501 ± 0.020) relative to $^{133}Cs/^{136}Ba$ of the interuraninite Ru, which are less than the expected fission yield (Fig. 5). The overabundance of $^{135}Ba^*$ (as live $^{135}Cs^*$) relative to $^{138}Ba^*$ indicated that Cs was more efficiently lost from the uraninite and able to be captured by the intergrain Ru. Conversely, the overabundance of $^{138}Ba^*$ in the Ru inclusion relative to both $^{135}Ba^*$ and other Ru aggregates indicated that fissionogenic Ba was retained more efficiently within the uraninite. Fractionation due to Ru formation is difficult to account for without another secondary mineral phase for comparison. We conclude, however, that the fractionation, or relative loss, of Cs/Ba from the uraninite lies in the range of 1.2–2.4. The similar $^{135}Ba^*/^{136}Ba$, $^{137}Ba^*/^{136}Ba$, and $^{133}Cs/^{136}Ba$ ratios in the inclusion, matching fission yields, further show that these isotopes behaved predominantly as Cs before formation, with little fractionation between them.

Discussion

While the Oklo phenomenon has been widely investigated for several decades, the application of new technology has yielded immediate discoveries. The NRL NAUTILUS micrometer-scale, molecule-free imaging capability enabled the identification of trace isotope concentrations in highly heterogeneous materials, which we believe to be the only accelerator mass spectrometry (AMS) imaging capability for electropositive elements. These measurements by conventional SIMS were obscured due to large molecular backgrounds and nonnormal isotopic compositions.

We made direct measurements of U isotopes, fission products, and n-capture products, which were not possible by conventional SIMS. We found the world's most depleted natural U and identified burnup depletions in Sm, Eu, Gd, and Dy in situ. RZ 13 appears to be a special RZ, being well preserved deep underground and having experienced the highest neutron fluxes over a shorter period of time than other reactors (3, 4). We discovered that Ru metal and sulfides were collocated with fissionogenic Cs and Ba, which was captured 5 y following reactor shutdown. Furthermore, these radioactive fission products were captured in the most active region of all Oklo reactors. Understanding the release and sequestration of specific radiogenic signatures into the environment is important, and this discovery provides insight toward long- and short-term nuclear-waste moderation strategies. Whereas most fissionogenic Ba and Cs were lost from the reactor, Ru captured and held the fission products for 2 Ga following reactor shutdown, with the intrusion of a dolerite dike likely caused loss of ^{133}Cs ∼1 Ga following reactor shutdown. Cesium appears to be more efficiently lost from the reactor fuel than Ba, but at least as efficiently captured by Ru metal and sulfides. It would be of great interest to know whether similar Ru–Cs–Ba correlations are present in Ru aggregates from other RZs and whether the Ru phase (e.g., metal, oxide, or sulfide) affects Cs and Ba capture and retention. Nanoscale transmission electron microscopy could illuminate the bonding differences of Cs relative to Ba in Ru metal/sulfides. The natural nuclear reactor samples from Oklo and Bangombé have provided a wealth of information over the decades regarding the migration and storage of fission products, and based upon recent findings, further investigation is warranted.

Methods

A description of the NAUTILUS instrument is provided in refs. 14–16, but at its most basic level, it can be understood as a SIMS instrument with an additional AMS "detector," which removes molecular isobars. SIMS and AMS are otherwise well known commercial capabilities. O^- and O_2^- probes between 100 pA and 1 nA were used to perform imaging and spot measurements. See *SI Appendix* for further details.

ACKNOWLEDGMENTS. We thank Maurice Pagel (University of Paris) for providing this extraordinary Oklo sample. We thank Kim Knight (Lawrence Livermore National Laboratory) for helpful discussions. This work was supported by Basic Research funding from the Office of Naval Research through NRL.

1. Bodu R, Bouzigues H, Morin N, Pfiffelmann JP (1972) Sur l'existence d'anomalies isotopiques recontrees dans l'uranium du Gabon. *C R Acad Sci Paris* 275:1731–1734.
2. De Laeter JR, Hidaka H (2007) The role of mass spectrometry to study the Oklo-Bangombé natural reactors. *Mass Spectrom Rev* 26:683–712.
3. Gauthier-Lafaye F, Holliger P, Blanc PL (1996) Natural fission reactors in the Franceville basin, Gabon: A review of the conditions and results of a "critical event" in a geologic system. *Geochim Cosmochim Acta* 60:4831–4852.
4. Hidaka H, Holliger P (1998) Geochemical and neutronic characteristics of the natural fossil fission reactors at Oklo and Bangombé, Gabon. *Geochim Cosmochim Acta* 62:89–108.
5. Ruffenach JC, Menes J, Devillers C, Lucas M, Hagemann R (1976) Etudes chimiques et isotopiques de l'uranium, du plomb et de plusieurs produits de fission dans un echantillon de minerai du reacteur naturel d'Oklo. *Earth Planet Sci Lett* 30:94–108.
6. Meshik AP, Hohenberg CM, Pravdivtseva OV (2004) Record of cycling operation of the natural nuclear reactor in the Oklo/Okelobondo area in Gabon. *Phys Rev Lett* 93:182302.
7. Dymkov Y, Holliger P, Pagel M, Gorshkov A, Artyukhina A (1997) Characterization of a La-Ce-Sr-Ca aluminous hydroxy phosphate in nuclear zone 13 in the Oklo uranium deposit (Gabon). *Miner Depos* 32:617–620.
8. Meshik AP, Kehm K, Hohenberg CM (2000) Anomalous xenon in zone 13 Okelobondo. *Geochim Cosmochim Acta* 64:1651–1661.
9. Brookins DG, Lee MJ, Mukhopadhyay B, Bolivar SL (1975) *Search for Fission-Produced Rb, Sr, Cs and Ba at Oklo* (International Atomic Energy Agency, Vienna).
10. Hidaka H, Konishi T, Masuda A (1992) Reconstruction of cumulative fission yield curve and geochemical behaviors of fissiogenic nuclides in the Oklo natural reactors. *Geochem J* 26:227–239.
11. Ewing RC (2015) Long-term storage of spent nuclear fuel. *Nat Mater* 14:252–257.

12. Beresford NA, et al. (2016) Thirty years after the Chernobyl accident: What lessons have we learnt? *J Environ Radioact* 157:77–89.
13. Koo Y-H, Yang Y-S, Song K-W (2014) Radioactivity release from the Fukushima accident and its consequences: A review. *Prog Nucl Energy* 74:61–70.
14. Fahey AJ, Groopman EE, Grabowski KS, Fazel KC (2016) Measurement of uranium isotopes in particles of U3O8 by secondary ion mass spectrometry-single-stage accelerator mass spectrometry (SIMS-SSAMS). *Anal Chem* 88:7145–7153.
15. Grabowski KS, Groopman EE, Fahey AJ (2017) Enhanced spatially-resolved trace analysis using combined SIMS–single-stage AMS. *Nucl Instrum Methods Phys Res Sect B* 410:41–46.
16. Groopman EE, Grabowski KS, Fahey AJ, Koop L (2017) Rapid, molecule-free, in situ rare earth element abundances by SIMS-SSAMS. *J Anal At Spectrom* 32:2153–2163.
17. Richter S, et al. (2010) New average values for the n(238U)/n(235U) isotope ratios of natural uranium standards. *Int J Mass Spectrom* 295:94–97.
18. Loss RD, et al. (1988) The Oklo natural reactors: Cumulative fission yields and nuclear characteristics of Reactor Zone 9. *Earth Planet Sci Lett* 89:193–206.
19. Holliger P, Devillers C (1981) Contributionàl'étude de la température dans les réacteurs fossiles d'Oklo par la mesure du rapport isotopique du lutétium. *Earth Planet Sci Lett* 52:76–84.
20. Hidaka H (1999) Isotopic study of natural fission reactors at Oklo and Bangombe, Gabon. *J Radioanal Nucl Chem* 239:53–58.
21. Crozaz G, Zinner E (1985) Ion probe determinations of the rare earth concentrations of individual meteoritic phosphate grains. *Earth Planet Sci Lett* 73:41–52.
22. Fahey AJ (1998) Details of the measurement of rare earth and other trace element abundances by secondary ion mass spectrometry. *Int J Mass Spectrom* 176:63–76.
23. Zinner E, Crozaz G (1986) Ion probe determination of the abundances of all the rare earth elements in single mineral grains. *Int J Mass Spectrom Ion Process* 69:17–38.
24. Shibata K, et al. (2011) JENDL-4.0: A new library for nuclear science and engineering. *J Nucl Sci Technol* 48:1–30.
25. Hidaka H, Gauthier-Lafaye F (2008) Ba isotopic signature for early differentiation between Cs and Ba in natural fission reactors. *Geochim Cosmochim Acta* 72:4123–4135.
26. Hidaka H, Holliger P, Masuda A (1993) Evidence of fissiogenic Cs estimated from Ba isotopic deviations in an Oklo natural reactor zone. *Earth Planet Sci Lett* 114:391–396.
27. Donohue PC, Katz L, Ward R (1965) The crystal structure of barium ruthenium oxide and related compounds. *Inorg Chem* 4:306–310.
28. Donohue PC, Katz L, Ward R (1966) The modification of structures of ternary oxides by cation substitution. I. Substitution of strontium for barium in barium ruthenium oxide and in barium iridium oxide. *Inorg Chem* 5:335–338.
29. Donohue PC, Katz L, Ward R (1966) The modification of structures of ternary oxides by cation substitution. II. Substitution of various cations for ruthenium in barium ruthenium oxide. *Inorg Chem* 5:339–342.